Amorphous phosphorus: A cluster-network model

D. Hohl*
National Center for Supercomputing Applications, University of Illinois at Urbana-Champaign, Urbana, Illinois 61801

R. O. Jones
Institut für Festkörperforschung, Forschungszentrum Jülich, D-5170 Jülich, Federal Republic of Germany
(Received 22 July 1991)

We have performed an extensive theoretical investigation of amorphous phosphorus (a-P) using the molecular-dynamics–density-functional method. The energy surfaces and forces for 124 atoms in a constant-volume simple cubic cell were calculated using the density-functional formalism, with a local-density approximation for the exchange-correlation energy. Pair correlation functions $g(r)$, structure factors $S(Q)$, phonon densities of states, ring statistics, and various static distribution functions (including distributions of bond and pyramid angles) were computed and compared with experimental and theoretical data where available. Although amorphous solids are usually likened to crystalline polymorphs with known structures, we find that the structure of rapidly quenched a-P resembles a network of small P_n clusters more than any of its common crystalline allotropes.

I. INTRODUCTION

The determination of the structures of amorphous materials is a fundamental problem of condensed-matter physics. It has been studied with various experimental techniques for many years, including x-ray and neutron diffraction, extended x-ray-absorption fine structure (EXAFS), Raman scattering, and infrared (ir) spectroscopy. It is rare for a single experiment to lead to an explicit disordered structure, and a combination of various experiments and theoretical studies is usually necessary. It is not surprising that the result can be contradicting structural models, even in one-component elemental amorphous materials like Se,[1] As,[2] P, and Si. An inherent difficulty in these materials is the quasistability and a significant dependence of the microscopic structure and many properties on preparation method and subsequent treatment.

In the present work we study amorphous phosphorus, which is an important amorphous wide-gap semiconductor with interesting properties beyond its use as a n-type dopant in the semiconductor industry. Examples are photodarkening, other light-induced changes like photoenhanced vaporization[3] and radiative recombination phenomena investigated extensively with time-resolved photoluminescence,[4,5] and optically detected magnetic resonance.[6] These phenomena are often linked to intrinsic coordination defects P_4 and P_2 (Ref. 7) and their "negative-U" or "positive-U" character.[8] As a group-Va element with valence electronic configuration s^2p^3, phosphorus is threefold coordinated in all its low-pressure condensed elemental forms,[9] but it can occur with coordination numbers 2,[10] 3, 4 (e.g., the PO_4 group in phosphates), and 5 (e.g., PCl_5) in small clusters and chemical compounds. Intermediate between its group-IVa (Si,Ge) and group-VIa neighbors (S,Se), the structural chemistry and reactive behavior of P are very similar to those of its heavier and slightly larger[11] analog As,[9,12–14] and many conclusions of this work should also apply to amorphous As.

In an elemental form, phosphorus shows a structural variety exceeded only by sulphur and possibly boron, and there have been many studies of the crystalline forms.[9,15] *White phosphorus* in the liquid and solid form consists of tetrahedral P_4 molecules (bond distance $d = 2.21$ Å, bond angle $\alpha = 60°$). The crystalline α and β modifications have not been fully characterized[16] and are probably rotationally disordered plastic crystal phases. *Orthorhombic black phosphorus* (o-P) consists of puckered double layers of identical sixfold rings[9] ($d = 2.22$ and 2.24 Å, $\alpha = 96°$ and 102°) and is the stable allotrope under standard conditions. When subjected to pressures above 12 kbar, o-P transforms to the *black rhombohedral* modification (r P), with a sheet structure comprising identical sixfold rings ($d = 2.13$ Å, $\alpha = 105°$), and then to a *simple cubic* structure (c-P) with increased coordination number 6 ($d = 2.38$ Å).[9] The most stable allotrope of As has the same crystal structure as r-P. *Monoclinic ("Hittorf's", violet) phosphorus* (m-P) has 84 atoms in the unit cell and requires a special preparation procedure[17] starting from white phosphorus. It consists of layers of parallel tubes of pentagonal cross section containing cagelike P_8 and P_9 clusters. The tubes in adjacent layers are approximately perpendicular. The range of bond distances ($d = 2.18 - 2.30$ Å) and bond angles ($\alpha = 85° - 116°$) is considerably larger than for the other crystalline allotropes. Unlike the other crystalline polymorphs, the intermediate-range order (IRO) of m-P is formed by subunits we have identified as particularly stable isomers of small P clusters in previous molecular-dynamics–density-

functional (MD-DF) calculations.[10] Networks of P_n clusters other than P_8 and P_9 might have similar stability. We note here that inelastic neutron scattering[18] and Raman spectroscopy[19] measurements on glassy P_xSe_{1-x} indicate the existence of molecular clusters, predominantly P_4Se_3.

The microscopic structure of amorphous phosphorus has been studied extensively,[17,20–25,27,28], and two contradicting structural models based on known crystalline polymorphs have emerged: (i) *a*-P consists of layers similar to those in *o*-P. This model was developed on the basis of x-ray-diffraction experiments[21] showing close similarity between the radial distribution functions $J(r)$ deduced for *a*-P and *o*-P, with particular reference to the small third peak in $J(r)$. Further support comes from x-ray spectroscopy of *o*- and *a*-P in comparison,[29] ^{31}P nuclear magnetic resonance (NMR) (which probes short-range order),[30] and to a lesser extent from vibrational measurements.[23,24] The last emphasize the sensitivity of the IRO to preparation conditions, and indicate distinct differences between bulk *a*-P and gas-phase deposited films. The results show qualitative similarity to As,[31,32] and have been explained in a layerlike model. (ii) *a*-P consists of tubes of pentagonal cross section as in *m*-P. This was the conclusion of x-ray diffraction derived $J(r)$ diagrams,[17,20] Raman-scattering experiments[26,25] and most convincingly of recent inelastic neutron scattering experiments on *m*-, *o*-, and *a*-P.[33] In a subsequent comparative Raman study of *m*-, *o*-, bulk *a*- and thin-film *a*-P deposited under varying conditions, Olego, Baumann, and Schachter[27] found indications that both models are plausible, the faster quenched films resembling double layers as in *o*-P and the more slowly quenched films resembling bulk *a*-P and *m*-P. By contrast, random network models[2,28] have difficulties in reproducing experimental data for *a*-P, and an accurate description of the chemical bonding in covalent pnictide materials seems essential for a good representation.

A density-functional calculation of saturated clusters of phosphorus (e.g., $P_{36}H_6$) has been performed by Briddon and Jones,[34] with particular focus on defect structures. However, to the best of our knowledge, no attempt has yet been made to use a MD simulation to generate *a*-P structures and develop structural models. We describe here such a study using the MD-DF method of Car and Parrinello.[35,36] This method avoids the bias of MD methods that employ empirical interatomic potentials, and it has proven to describe bonding and dynamics in covalent main group element systems very well.[1,14,35,37–45]. The method[38] and an application to phosphorus clusters[10,11] P_2–P_9 have been described previously, and only the details of the computations are given here.

II. COMPUTATIONAL DETAILS

Linewidth and intensity of the first sharp diffraction peak (FSDP) in *a*-P suggest a long structural correlation length[24] ($\geq$12 Å). We have therefore chosen a relatively large simple cubic unit cell with lattice constant $a = 14.35$ Å containing 124 P atoms. We use periodic-boundary conditions and the density ($\rho = 2.16$ g cm^{-3}) of bulk red *a*-P.[15] The 310 occupied electronic states ψ_i were expanded in a plane-wave basis set with cutoff energy 10.6 Ry at a single point in the Brillouin zone ($\mathbf{k}$=0). The nonlocal pseudopotential of Bachelet, Hamann, and Schlüter[46] with $l_{\max} = 1$ ("*s* nonlocality") was used in this work. In our earlier work on phosphorus clusters,[10] we showed that this approximation led to P-P bond distances about 1.5% longer than calculations with $l_{\max} = 2$, without otherwise affecting the very satisfactory description of the energy surfaces. In the cluster work, bond distances for P_2 and P_4 agreed with experimental data to better than 0.5%, and atomization energies were overestimated by about 1 eV/atom. A uniform overestimate of that size is common in applications of the local-density approximation (LDA), but binding energy trends, shapes of energy surfaces, and relative depths of different minima are given reliably.[47] With physical masses for the P atoms and a fictitious mass $\mu = 500$ a.u. for the electronic degrees of freedom ψ_i, the coupled equations of motion[35] could be solved accurately with a Verlet integrator and a time step $\Delta t = 9$ a.u. (2.2×10^{-16} s).

In order to generate representative low-lying amorphous structures and MD trajectories, the 124 atoms were initially placed on simple cubic lattice sites, with sixfold-coordinated atoms at nearest-neighbor distances of 2.9 Å. In order to break the lattice symmetry, all atoms were then displaced in all three space directions by a random distance between 0 and 0.7 a.u. For this geometry, we determined those ψ_i that minimize E, using an efficient self-consistent iterative diagonalization technique, such as described by Štich *et al.*[48] With the electrons initially in their ground state, the MD-DF dynamics[35] generate Born-Oppenheimer trajectories without requiring additional diagonalization and/or self-consistency cycles for the electrons over several thousand time steps. During the microcanonical MD runs, the maximum deviation from the ground-state energy of the system of 620 electrons was ~0.1 eV. To achieve this level of convergence, it was necessary to quench the electronic subsystem every few thousand time steps.

Figure 1 shows the total thermal treatment the MD system received. The trajectory can be decomposed into four phases: (1) Melting at temperatures up to $\sim$ 2200 K and annealing to 300 K. This phase lasted $\sim 8000\Delta t$, during which every P atom moved an average of 2.6 Å, more than a typical bond length. The cooling rate was $\sim 1.5 \times 10^{15}$ K/sec. (2) Equilibration at 300 K and first microcanonical trajectory ($\sim 5500\Delta t$). (3) Reheating to $\sim$ 1100 K and annealing to 300 K. This phase lasted $\sim 9500\Delta t$, the cooling rate was $\sim 5.5 \times 10^{14}$ K/sec and the atoms moved a further 1.9 Å on average. (4) Equilibration at 300 K and a second microcanonical trajectory ($\sim 5000\Delta t$). The total length of the trajectory was $\sim$ 6 ps and the microcanonical MD trajectories used for averaging were about 1.1 ps long. Short trajectories due to the large computational effort form a well-known limitation of MD-DF simulations in condensed-matter systems (one time step takes about 40 sec of Cray Y-MP CPU time). We have addressed this problem by employing a second annealing cycle and analyzing the subsequent structural changes. The average potential energies $\langle E_{\rm pot} \rangle$ in trajec-

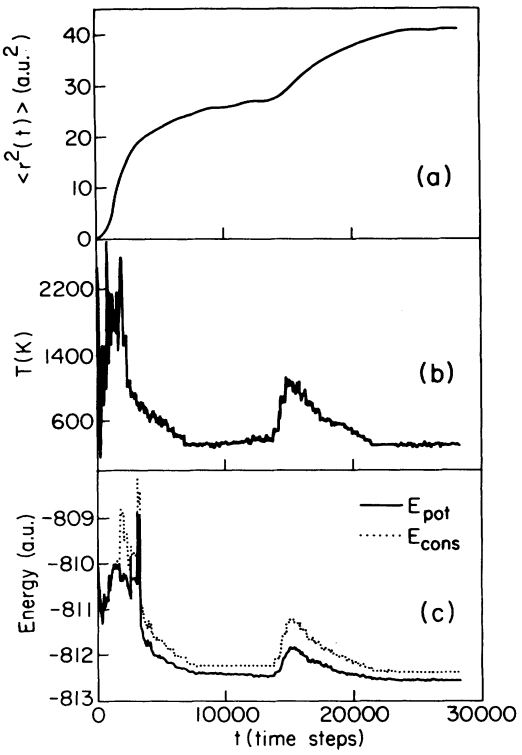

FIG. 1. Thermal history of the sample of 124 P atoms in the MD simulation. (a) Mean-square displacement $\langle\sum_i[\mathbf{r}_i(t)-\mathbf{r}_i(0)]^2\rangle$. (b) Temperature T (K) defined as average kinetic energy of the ions. (c) Classical potential and total energies E_{pot} and E_{cons}; E_{cons} is the sum of the ionic kinetic and potential energies, excluding the small kinetic energy of the electronic degrees of freedom. Two different microcanonical trajectories were computed with $T \sim 300$ K ("trajectory 1" and "trajectory 2"), with an intermediate annealing cycle.

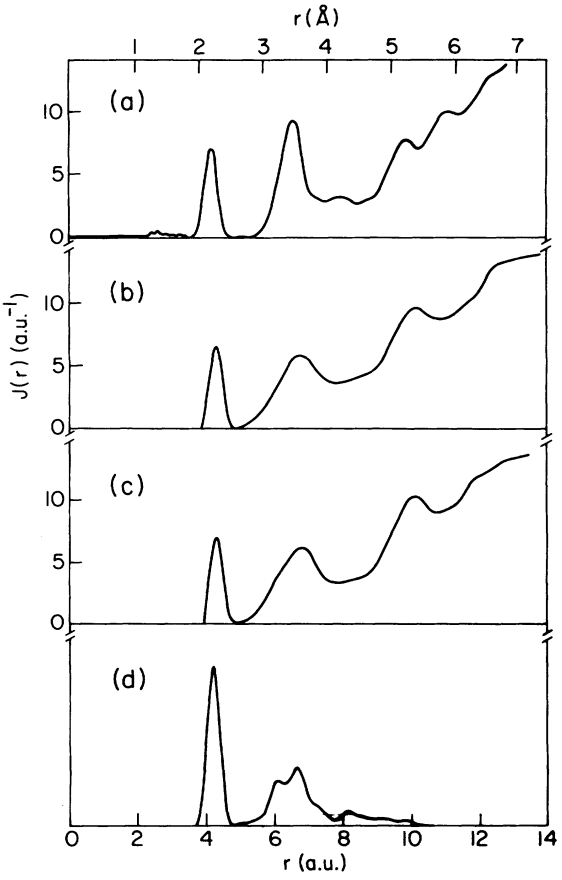

FIG. 2. Radial distribution functions $J(r) = 4\pi r^2 \varrho(r)$ obtained (a) from experiment (Ref. 28), (b) from MD trajectory 1, and (c) from MD trajectory 2 for amorphous phosphorus. The MD data are broadened with the experimental resolution for proper comparison. (d) shows the RDF histogram (in arbitrary units) derived from the geometries of 70 low-lying P_n structures ($n = 3-10$) in our previous MD-DF cluster study (Refs. 10 and 49). The diameter of the largest clusters included (about 5 Å) limits the graph on the high r side.

tories 1 and 2 differ by ~3 eV for the entire system so that the annealing served well the purpose of reaching a lower region of the energy surface.

III. RESULTS AND DISCUSSION

We now compare the data obtained from averaging over the two microcanonical trajectories with an elastic neutron-scattering study[28] on bulk a-P and other experimental data, with the crystal lattices of r-, o- and m-P, and with a set of 70 low-lying P_n ($n = 4$–10) structures from our cluster MD-DF study.[10,11] The structures we have chosen for this purpose represent local minima in the energy surface within 2 eV of the calculated ground state.

A. Radial distribution and structure factor

Figure 2 shows the radial distribution function (RDF) of bulk a-P as deduced from experiment[28] and MD trajectories 1 and 2. Both experiment and calculations show three clearly distinguishable peaks at distances d_1, d_2, and d_4 (see first two columns of Table I). The $J(r)$ histograms compiled from the MD data also show distinguishable structure at d_3 that, when broadened with the experimental resolution,[28] becomes almost invisible in Figs. 2(b) and 2(c). The calculated peak positions agree well with experiment, with a shift to larger r of about 1–2% consistent with the use of s nonlocality in the pseudopotential. Although the overall shape of the diagrams is in good agreement, there are characteristic differences between theory and experiment: The second peak in $J(r)$ is less intense and broader in the calculations, the structure between second and third peak is underdeveloped, and only the first maximum of the characteristic three-peak signature between 5 and 7 Å is well developed. The last feature is not surprising, since the boundaries of the MD cell are approached, and there are even considerable differences between different experiments in this region.[20,21,28] The first two are not nec-

TABLE I. Interatomic distances d_n (in Å) in the nth neighbor shell of bulk a-P, and a-P from the present calculations, and in crystalline r-, o- and m-P. The corresponding coordination numbers are given in parentheses where available.

	Bulk a-P	a-P[a]	r-P[b]	o-P[b]	m-P[c]
d_1	2.24 (2.97[d])	2.27 (3.0)	2.13 (3)	2.23 (3)	2.22[e] (3)
d_2	3.48[d] (7.7[f]; 8-11[g])	3.55 (10.8)	3.34[e] (3+6)	3.40[e] (8), 3.70[e] (4)	3.46[e] (8.24)
d_3	4.3[d] (2-3[g])	~4.4 (~ 2)		3.99, 4.25, 4.38	3.97, 4.13, 4.50
d_4	5.3[d]	5.4 (~ 20)			4.83, 5.18

[a]This work. Peak positions in $g(r)$ are identical for trajectories 1 and 2.
[b]Reference 9.
[c]Reference 17.
[e]Average value.
[d]Reference 28.
[f]Reference 20.
[g]Reference 21.

essarily inadequacies of the calculations, but also reflect the variations of the material with preparation conditions. The sample used in the neutron-scattering experiment was thermally prepared from white phosphorus[28] and thus well annealed, while our MD prepared sample was quenched very rapidly (see Sec. II).

If we compare $J(r)$ from trajectories 1 and 2 (see Fig. 1), we find that the region most affected by the additional annealing cycle is indeed the second peak at 3.55 Å and the neighboring first and second minima. The second peak draws weight from those minimum regions and develops a visible shoulder around 3.3 Å with the second minimum region gaining structure near 4.4 Å. The three peaks between 5 and 7 Å become sharper and more clearly developed, and the overall agreement with the experimental curve is improved (Fig. 2). An asymmetric second peak is also found in the experimental $J(r)$ curve [see Fig. 2(a)] and has been taken as evidence for an asymmetric or bimodal bond angle distribution $A(\alpha)$.[28] The structure and origin of the peaks will be discussed in detail below in conjunction with the results of our cluster study.

Bulk a-P shows a pronounced low-angle diffraction peak ("prepeak," FSDP) at $Q \sim 1$ Å^{-1}. Similar peaks occur in a-As, a-Se, and the chalcogenide glasses. They are usually taken as evidence of IRO in glasslike materials. It has been shown[23,24] that its intensity decreases greatly from the bulk a-P value in a-P films deposited at surface temperatures below 350–400 K. Peak intensity was therefore interpreted as measure of interlayer correlations in a layerlike model. We have computed the structure factor $S(Q)$ by Fourier transforming the pair correlation function $g(r)$ and compare our results with the experimental curve in Fig. 3. The agreement between the curves in peak positions and intensities is excellent, with the expected small redshift at higher Q values due to the overestimation of bond distances explained above. The FSDP is clearly visible in the correct position in the theoretical curve but much smaller in intensity than for the experimental curve. We observe an increase in intensity from trajectory 1 to trajectory 2 of 25%. The intensity mismatch can therefore be attributed to the fast-quenching procedure in the MD sample when compared to well-annealed bulk a-P. a-As, for which only a layerlike model analogous r-(P,As) is popular, shows an experimental FSDP about as small in intensity as we derive for a-P from MD.[31]

Fourier back-transform and modeling studies have shown that all essential features of $S(Q)$ in a-As can be reproduced when one considers a neighbor shell of radius *not more* than 12 Å.[31] On the other hand, a combination of x-ray diffraction and Raman-scattering studies was interpreted with a structural correlation length of *not less* than 12 Å in bulk a-P.[24] We have found that $S(Q)$ remains qualitatively unchanged when we truncate the Fourier transform of $g(r)$ at distances as low as $r_{FT} = 4.8$ Å. Lowering r_{FT} even further leads to dramatic changes in the first and second peak regions of $S(Q)$, and the FSDP near 1 Å^{-1} disappears completely with $r_{FT} \lesssim 4.1$ Å. We conclude that the first two peaks and minima in $g(r)$ contain all information that leads to an FSDP near 1 Å^{-1} in fast quenched a-P and very likely in a-As.

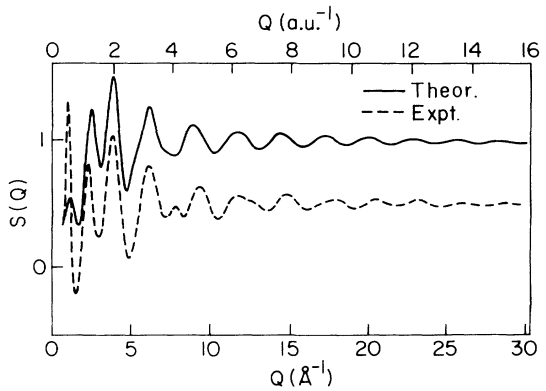

FIG. 3. Comparison of theoretical and experimental (Ref. 28) static structure factors $S(Q)$ for a-P. The experimental curve has been shifted by −0.5. The theoretical curve is from trajectory 2.

As noted in Ref. 24, very long-range structural correlations may be present in (much more slowly annealed) bulk a-P, but they are not necessary for an FSDP in that Q range. In particular, one need not invoke "interlayer" or "intertube" spacings.[26] The intermediate MD annealing cycle between trajectories 1 and 2 does not influence $S(Q)$ dramatically, but the overall agreement with the experimental curve is better (e.g., the appearance of leading and trailing shoulders of the fourth peak at 6 $Å^{-1}$). The good qualitative agreement between experimental and theoretical $J(r)$ and $S(Q)$ indicates that we can proceed with an analysis of quantities that are not experimentally accessible.

It is evident from Table I that no model for a-P based on crystalline polymorphs can be favored simply on the basis of (theoretically or experimentally derived) interatomic distances and coordination numbers. The different crystalline forms of P are too similar, and the experimental resolution is too small for a-P. Compiling $g(r)$ statistics (see Fig. 2) from our data base of 70 P_n cluster structures, we found that the characteristic pattern found in a-P (sharp symmetric first peak around 2.2 Å, asymmetric broader maximum around 3.4 Å, small third peak slightly above 4 Å) is universal to all forms of P, including small clusters [Fig. 2(d)] and therefore a property of the energy surface.[49] The analysis is easiest and most illuminating in small clusters, and we have used molecular graphics tools to identify the origin of the $g(r)$ patterns in Figs. 2(b)–2(d). We shall show that the existence of layers as in o-P or tubular objects as in m-P are not required for a detailed explanation.

The *first* peak near $d_1 = 2.2$ Å is naturally due to the covalently bonded first neighbors. It is broadened by the frequent occurrence of twofold-coordinated atoms in the smaller P_n clusters ($n \leq 7$) with shorter bonds and various conformations with elongated bonds.[10] Peak shape and width are virtually identical in our a-P samples [Figs. 2(b) and 2(c)], and thermal motion adds little broadening. The *second* maximum in Fig. 2(d) centered near 3.4 Å is very similar to the corresponding peak in Fig. 2(c) [slow onset far in the first minimum of $J(r)$, shoulder around 3.2 Å, maximum height at 3.5 Å, slow fall to second minimum in $J(r)$ near 4.1 Å with shoulder at 3.8 Å], but shows more structure. In the cluster case [Fig. 2(d)], there is a simple explanation for such a distinct pattern: Most of the second maximum is made up of next-nearest neighbors, with a multimodal bond-angle distribution $A(\alpha)$ [$\alpha = 91°$, 105°, and 120°, see below and Fig. 5(c)] leading to increased weight at interatomic distances $d_2 = 2d_1 \sin(\alpha/2)$ ($d_2 \sim 3.2$, 3.5, and 3.8 Å).

An identical explanation holds for the structure of the second maximum in our a-P samples. m-P also shows a doubly peaked second maximum in $g(r)$ (Fig. 9 in Ref. 17) as consequence of a bimodal bond-angle distribution. Between 3.25 and 3.85 Å next-nearest- and third-nearest-neighbor distances overlap significantly; the *third* maximum in Fig. 2(d) at $d_3 = 4.3$ Å eventually consists exclusively of third-nearest neighbors. The relative maximum of $g(r)$ at $r = d_3$ can be attributed to the frequent occurrence of strings of four bonded atoms with dihedral angles γ between 80° and 110°. Although the dihedral angle distribution function $D(\gamma)$ (Ref. 1) does not characterize threefold-coordinated materials very well (see below), it shows a clear maximum at 90° in the set of 70 P_n clusters considered, and the distance between the terminal atoms d(1-4) in bonded four-atom strings shows an almost linear correlation with γ. Other significant maxima of $D(\gamma)$ lie at lower angles ($\gamma \sim 60°$, 30°, and 0°) and the corresponding distances d(1–4) contribute to the second maximum region of $g(r)$. It is important to note that both o-P and m-P show identical maxima in $g(r)$ near d_3 and in $D(\gamma)$ near $\gamma = 80°$.

Much discussion has focused on the third maximum at d_3 in the *experimental* $J(r)$ diagram. The proponents of the o-P model have used the third-nearest neighbors within the P_6 rings in that allotrope at 4.01 Å and 4.24 Å as supporting their view.[21] Likewise, those who favor the m-P model point out a third maximum in $J(r)$ for that material with peaks at 3.95 Å and 4.13 Å.[17] Neither agrees perfectly in position with the experimental third maximum. It is interesting that the less than satisfactory agreement in the case of m-P is due mainly to the strong peak at 3.95 Å (at too low r). This is a distance *between* the P_8 and P_9 clusters and the P_2 units connecting those objects to tubes (i.e., distances between atoms 2–12, 4–10, 6–12, 4–14, 5–18, 6–16, and 8–14 in Fig. 2 of Ref. 17). A random network of P_8 and P_9 clusters would provide a better representation of the experimental $J(r)$ graph for a-P, and we have shown that clusters of other sizes can also be included.

In our previous MD-DF study of liquid and amorphous selenium,[1] we found that the fast-quenching procedure leads to an overestimation of coordination defect concentrations. Although it is possible to deduce an average number of first neighbors with good accuracy, it is difficult to estimate defect concentrations from any experiment. However, it has been suggested that twofold and fourfold coordinated atoms P_2 and P_4 will constitute the dominant defects[8] and made clear that the concentrations strongly depend on the preparation conditions.[4] Counting as bonded only atoms within a shell of 5.0 a.u. (first minimum in $g[r]$), we can easily give the percentage of coordination numbers N that leads to an overall coordination of 3.0 in our MD sample (see also Fig. 4):

N	Trajectory 1	Trajectory 2
1	0	0
2	13	10
3	80	83
4	7	6
5	0	1

This confirms the dominance of P_2 and P_4 defects and provides evidence that these two defect types are local minima and thermally stable at modest temperatures. Manually constructed, both isolated P_2 and P_4 defects and bonded P_2/P_4 defect pairs represented stable local minima in recent P_nH_m cluster calculations with a LDA method similar to ours.[34] The effect of the annealing cycle between trajectories 1 and 2 is not dramatic, but results in a noticeably lower concentration of P_2 and P_4. It is therefore clear that faster quenching will lead to higher

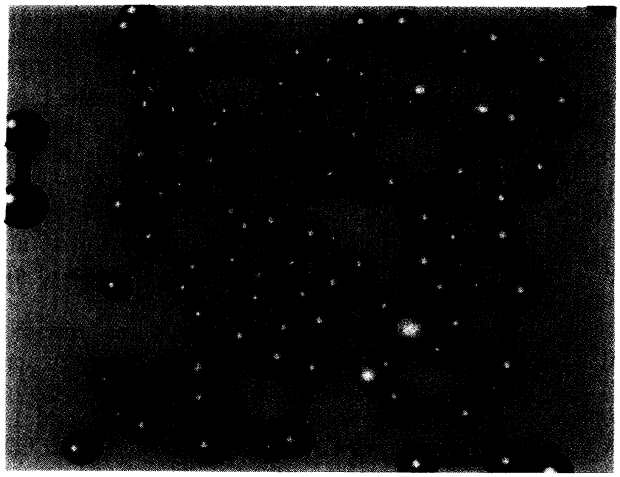

FIG. 4. Ball-and-stick model of a typical spatial configuration in a-P (trajectory 2). Twofold-coordinated defects are shown in red, fourfolds in yellow. All atoms inside the periodically repeated cube are shown and bonds are drawn between atoms within the cell with separation $d \leq 5.0$ a.u. Bonds to atoms in neighboring cells are omitted, so that the number of sticks is not necessarily a measure of the coordination number near the cell edges.

proportions of defects, but we cannot give reliable estimates for slowly annealed bulk a-P on the basis of our data. Although it may be assumed that those numbers lie lower, a MD study of a-Si employing a sophisticated empirical potential and $\sim$ 4 ns of thermal treatment[50] shows coordination defect concentrations very similar to those found here.

B. Bond angles

The distance between the first and second peaks in the experimental $J(r)$ function yields an average bond angle of $\alpha = 103°$ (Ref. 28) and the strong deviation from the Gaussian shape in the second peak suggests an asymmetric or multimodal bond-angle distribution $A(\alpha)$. The distribution function itself is experimentally not accessible in amorphous materials. Both crystalline m-P and o-P show bimodal distributions peaking at 98° and 105° and at 96° and 102°, respectively. Again, a distinction between models based on m- or o-P for a-P is difficult. In Fig. 5 we show the $A(\alpha)$ graphs for MD trajectories 1 and 2 and the corresponding statistics from the cluster calculations.[10] The sample before annealing in Fig. 5(a) shows a broad (standard deviation 20°), featureless maximum in A_3 around 103° and a much smaller feature at 60°. The MD annealing cycle sharpens the latter and adds more structure to the main peak in Fig. 5(b), which now appears to contain major contributions at 103° and 93° and a lesser one at 120°. Those at 103° and 93° are close in position and relative weight to those in o-P and similar to those of m-P (see above). The smaller features at 60° and 120° are incompatible with any crystalline polymorph. The former, in particular, is very characteristic, clearly stable against thermal treatment, and not an artifact of the fast quench preparation conditions. It has been observed in previous MD simulations of liquid As,[13,14] but its nature has not been identified.

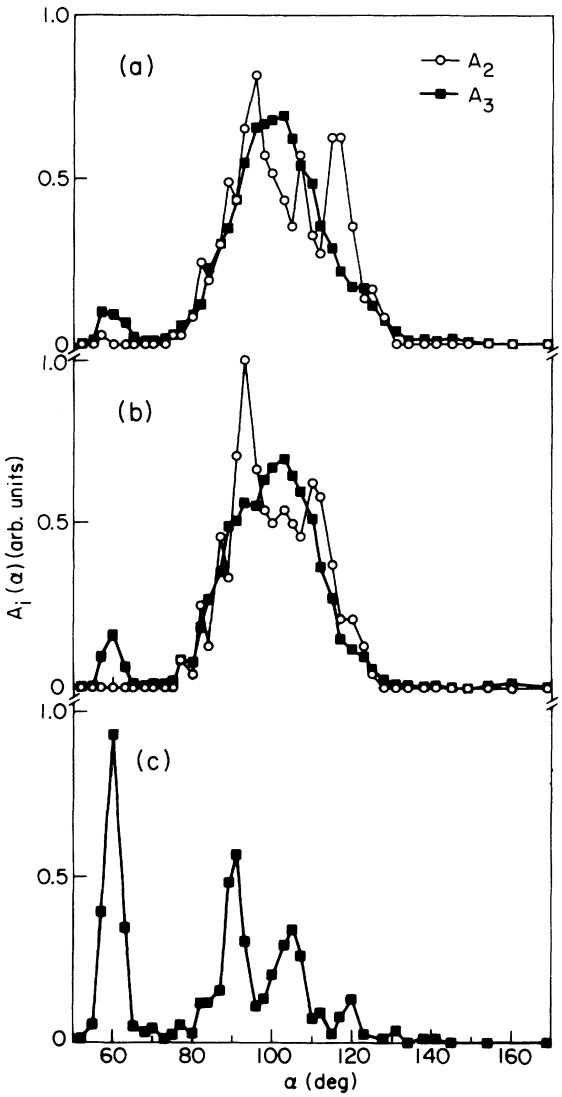

FIG. 5. Bond-angle distribution functions A_i for i-fold coordinated atoms in a-P. Trajectories 1 and 2 are shown in (a) and (b), respectively. A_3 from 70 low-lying P_n structures in our MD-DF cluster study (Ref. 10) is shown in (c). The first neighbor shell used to determine the coordination number has a radius of 5.0 a.u. in all cases. Varying this criterion between 4.3 a.u. and 5.0 a.u. did not have a visible effect on $A(\alpha)$. A_2 and A_3 are normalized to the same arbitrary number.

For comparison with the statistics in the condensed phase, we show in Fig. 5(c) the distribution of bond angles A_3 in the 70 cluster structures considered in Ref. 10. Clearly distinguishable peaks are evident at 60°, 91°, 105°, and 120°, and the positions of the maxima agree well with those in a-P. The preference for closed structures for P_n, even at small n where large bond angles

are not favored,[10] leads to decreasing peak heights with increasing α. The prevalence of $\alpha = 60°$ is due to the occurrence of nearly equilateral triangles P_3 and "roof" shaped P_4 clusters (two triangles with a common side) as building blocks in most of the P_n structures with $n \geq 5$. The same building blocks can be found in the MD sample, a typical view of which is shown in Fig. 6. The generation of tetrahedral P_4 objects is not favored and, contrary to an assumption made for ℓ-As,[13] we expect a similar situation in ℓ-As.

Peaks near 60° in the bond-angle distribution of other liquid and amorphous main group elements are not uncommon. They were identified in MD simulations of, e.g., a-Al,[51] ℓ-Al, and ℓ-Ga,[52] where attempts were made to explain the bond angle distributions with a close packing of highly symmetric subunits (polytetrahedra, icosahedra, fcc packing, etc.), without providing a detailed analysis of microscopic structures. For small Al_n clusters, Jones[53] showed recently that close packed structures and disordered open layer structures with triangular subunits can have comparable stabilities. ℓ-(Si,Ge) and a-Si also show (strong and weak, respectively) features in $A(\alpha)$ at 60° (Refs. 35 and 54) in conjunction with the expected peak near the tetrahedral angle 109°, and it is interesting to speculate whether all these findings can be explained without invoking crystalline or close packed highly symmetric subunits. We conclude that a doubly peaked bond-angle distribution between 90° and 100° is a universal property of the energy surface and coordination chemistry of P, and is therefore not very useful for identifying particular crystal-like phases. Furthermore (unlike o- and m-P), a mixture of small clusters exhibits the features at 60° and 120° observed in $A_3(\alpha)$ for a-P and might therefore constitute a better basis than crystalline models for understanding a-P at the microscopic level.

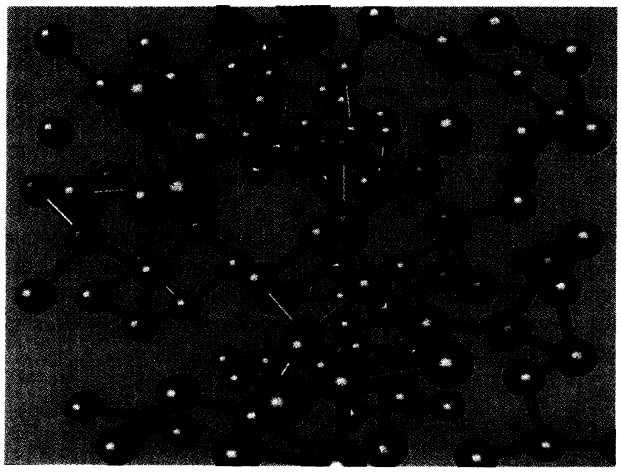

FIG. 6. Another view of the same configuration as in Fig. 4 from a similar angle. Atoms involved in near 60° bond angles are red, all others orange. Triangular P_3 and roof-shaped P_4 fragments and not P_4 tetrahedra are responsible for the peak at 60° in $A(\alpha)$.

C. P_4 pyramids and their orientation

The dihedral angles γ provide the most characteristic distribution function in twofold-coordinated glasses like Se,[1], where clear maxima and minima in $D(\gamma)$ allow a distinction between various models. However, it no longer provides a good characterization of threefold-coordinated materials like P. If we project along a bond between two threefold-coordinated P atoms, the following four rotational conformations occur in crystalline r-P (all bonds "full-trans"), o-P (1/3 of the bonds "half-trans," 2/3 full-trans) and m-P (with half-trans, "staggered," and "eclipsed" bonds[17])

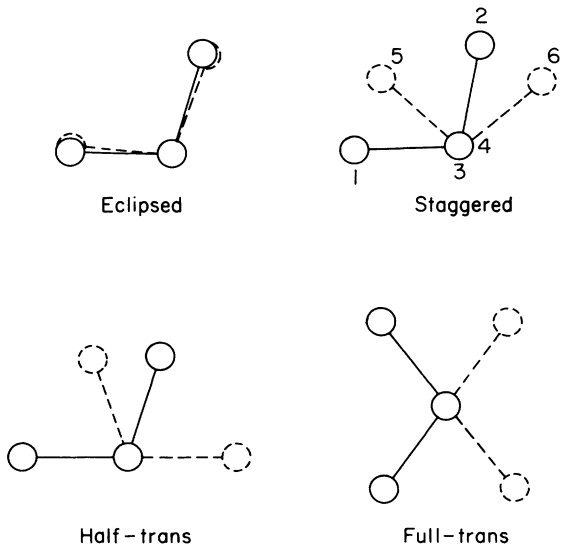

To describe these structures we have extended the notation used by Donohue.[9] In general, each of the conformations leads to four different dihedral angles at the central bond 3-4, and we can indeed observe all γ values between 0° and 180° in our MD generated a-P samples. Superimposed are distinguishable maxima at $\gamma \sim 0°, 30°, 60°, 90°$, and 180° (trajectory 2), but a possibly sharper maximum-minimum structure in the rotational conformations is lost. It is not easy to find a consistent and unambiguous measure of the angle ϕ describing the rotational conformation in the general case where all bond angles and bond distances may vary, and where atoms 1 and 5 and/or 2 and 6 may be identical (as is frequently the case in a-P). The concept of *pyramid angle* ϕ statistics used by Li in the MD simulation of ℓ-As[14] was found very useful here.

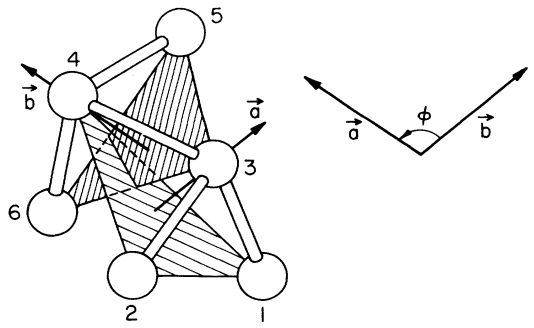

The angle between the two vectors **a** and **b** describes the relative orientation of the adjacent pyramids 1-2-4-3 and 3-5-6-4. When only the parts perpendicular to the axis 3-4 of **a** and **b** ($\mathbf{a}_\perp$ and $\mathbf{b}_\perp$, respectively) are considered, the angle $\phi_\perp$ between them recovers the description of rotational conformation as full-trans ($\phi_\perp = 180°$), half-trans ($\phi_\perp \sim 60° - 70°$), staggered ($\phi_\perp \sim 45°$), and eclipsed ($\phi_\perp = 0°$). By itself, however, this is not a useful measure in the general disordered case, when some terminal atoms 1 and 5 and/or 2 and 6 may be identical and all bond distances and angles can differ. Figure 7 compares the pyramid angle distribution $P(\phi)$ for both MD trajectories with the same statistics for our previous cluster study and for *m*- and *o*-P. The pyramids are obviously not randomly oriented in our P_{124} MD samples, Figs. 7(a) and 7(b). Trajectory 1 shows pronounced maxima at about $\phi = 180°$ and 140° and a broad featureless maximum at 60° ($\cos\phi = -1$, -0.77, and 0.5). The second annealing cycle [trajectory 2, Fig. 7(b)] results in additional peaks in $P(\phi)$ at 95° and 80° and deep minima at 110° and 0° ($\cos\phi = -0.1$, 0.2, -0.34, and 1, respectively). The latter minimum is to be expected for geometrical reasons. Comparison with Fig. 7(d) shows that $P(\phi)$ for *a*-P contains characteristics from *o*-P ($\phi = 180°$ and 88°) *and* *m*-P ($\phi \sim 45° - 90°$), and also from *r*-P (not shown; a single peak at 180°). Yet the structure we observe for *a*-P differs distinctly from all of those crystalline polymorphs. Above $\cos\phi \sim -0.4$ the $P(\phi)$ statistics for 70 low-lying clusters [Fig. 7(c)] provides by far the best agreement with trajectory 2. Figures 7(b) and 7(c) both show the sharp peak at $\sim 90°$ (where, for example, half-trans conformations and roof-shaped P_4 clusters lie) and both shape and position of the broader maximum at $\sim 85° - 35°$ (where staggered and eclipsed conformations lie) match almost exactly.

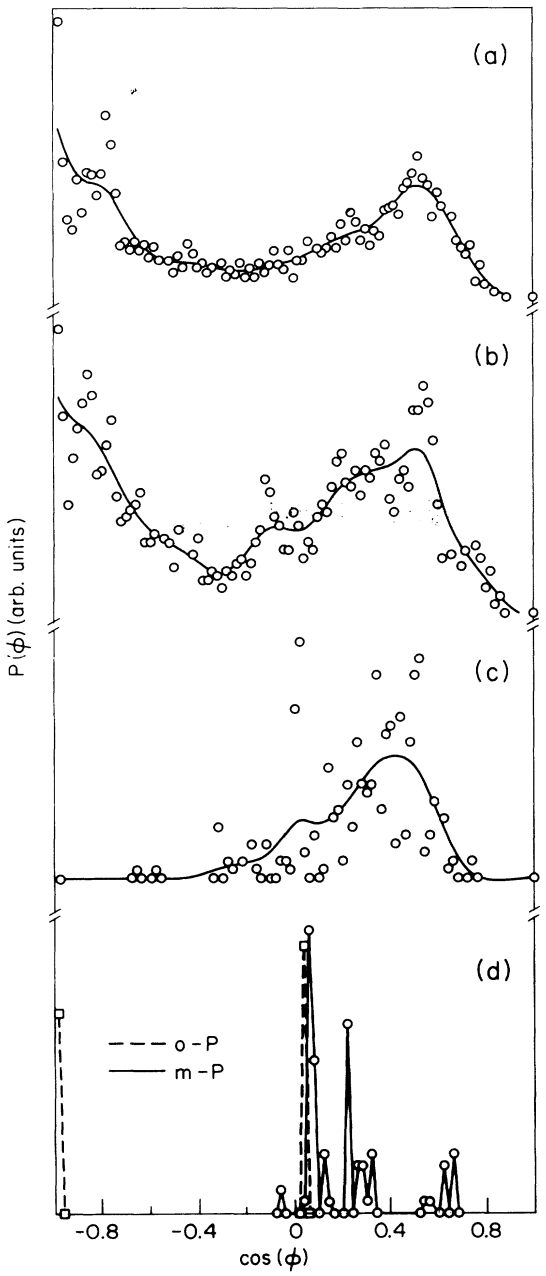

FIG. 7. Pyramid angle distribution $P(\cos\phi)$ for (a) trajectory 1, (b) trajectory 2 of our *a*-P MD simulation, and (c) 70 low-lying P_n structures from our previous MD-DF cluster study (Ref. 10). $P(\cos\phi)$ represents the temporal and cell average for the cosine of the angle ϕ between two P_4 pyramids bonded 5.0 a.u. or closer (see text). The histograms (redundant data points are omitted) are normalized to the same arbitrary number, and the lines are provided as a guide to the eye. (d) shows the corresponding histograms for *m*-P (solid line) and *o*-P (dashed line).

The maximum for *a*-P between 110° and 180° is not found in the cluster statistics. It corresponds to a preponderance of full-trans rotational conformations as in *o*-P and cannot be expected when compiling statistics from a manifold of unconnected clusters with only up to 10 atoms. Nearly full-trans conformations in closed P_n structures would require $n > 10$ (all open structures considered in Ref. 10 were found to be far above the ground state for all n investigated). They do, however, arise naturally when connecting smaller entities in an amorphous network (see Fig. 8). Finally, a comparison can be made with *ℓ*-As (Fig. 9 in Ref. 14), which was found to be very similar to the rhombohedral allotrope, with only one significant broad maximum at $\phi = 180°$. That calculation was also started with the As atoms on slightly perturbed simple cubic lattice sites, but the total thermal treatment was shorter (1 ps including melting and equilibration[55]) than ours for *a*-P. Our trajectory 1 in Fig. 7(a) has most weight near 180°, but the annealing process shifts weight to the $\phi \lesssim 90°$ region. Similar structural changes could occur upon further thermal treatment of *ℓ*-As, and it is not clear that the structural similarity with *r*-As is not a short-time artifact.

D. Rings as constituents

A MD cell with 124 atoms is large enough to derive reliable ring statistics, where a "ring" is defined as *any* closed path (or loop) through the network of atoms. Rings are constructed by starting from an atom and tracing a closed path of "bonds" [interatomic separation $\leq$ 5.0

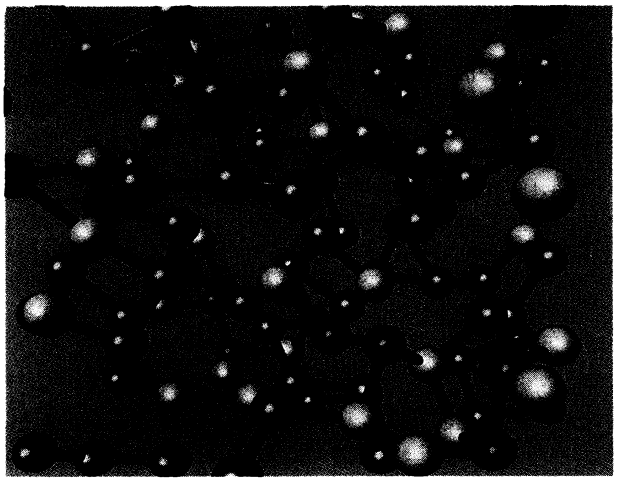

FIG. 8. Another view of the same configuration as in Fig. 4. All atoms connecting pyramids at angles $\phi = 160° - 180°$ are shown in red, the terminal atoms connected directly to those in yellow. Note the two closest full-trans conformations in the lower right-hand corner. Only the 124 atoms in the central unit cell are included.

a.u., the first minimum in $g(r)$], visiting no atom more than once. Rings may extend into neighboring unit cells, larger rings may comprise smaller units, and ring atoms are permitted to have bonds to more than two other ring atoms (e.g., the P_4 roof structure in Fig. 2 of Ref. 10 counts as two 3 rings and one 4 ring). Figures 6, 8, and 4 show typical views of the network encountered in the MD simulations. There is a variety of ring sizes and shapes, without a clear preference for any particular species (e.g., the chair-shaped 6 ring of crystalline r- and o-P). Rings of all sizes with $n \geq 3$ occur, and the distribution for both MD trajectories is shown in Table II up to $n = 11$. The annealing cycle between the two microcanonical trajectories generates more rings with $n \leq 8$ in trajectory 2 than in trajectory 1, another manifestation of the loss of memory of the starting configuration.

The most frequent ring sizes in the annealed trajectory (see Table II) are $n = 6$ and $n = 10$. In crystalline orthorhombic (and rhombohedral) phosphorus these would be the *only* ring sizes observed in the range $n \leq 11$ considered here (two 6-rings with a common side lead to $n = 10$). While six-membered rings appear to be particularly stable, a model based solely on six-membered constituents as in o-P does obviously not describe a-P well. Crystalline m-P contains rings with all $5 \leq n \leq 11$ when our definition is applied ($n = 5, 9$ being the most common), but three- and four-membered rings are absent. Since the latter increase in number upon further annealing, a model for fast-quenched a-P based purely on m-P and its P_8 and P_9 cages can be ruled out. Our choice of 70 particularly stable P_n cluster isomers cannot show rings with $n > 10$, since we compiled statistics only for isolated clusters up to P_{10}. However, all sizes $3 \leq n \leq 10$ occur, with a monotonic increase in frequency to $n = 6$ and a subsequent monotonic decrease to $n = 10$. Again, a description in terms of a network of small clusters seems more appropriate than a crystalline model for a-P.

TABLE II. Ring statistics. Average number N of n-fold rings in the 124 atom unit cell for MD trajectories 1 and 2. See text, Sec. III D.

	N	
n	Trajectory 1	Trajectory 2
3	4	5
4	7	11
5	16	19
6	17	24
7	11	14
8	13	19
9	25	23
10	26	26
11	25	21

E. Vibrational spectrum

In principle, MD simulations of disordered materials allow phonon densities of states (PDOS) to be determined

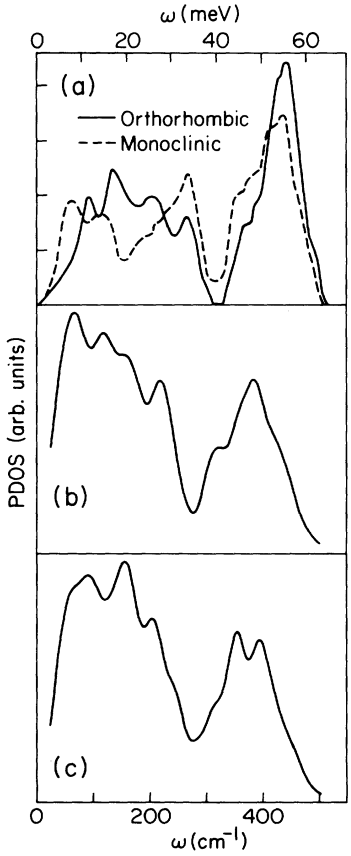

FIG. 9. Phonon density of states of (a) monoclinic and orthorhombic P [experiment (Ref. 33)], (b) MD sample before annealing (trajectory 1), and (c) MD sample after annealing (trajectory 2) in comparison.

from the Fourier transform of the velocity autocorrelation function $C_{vv}(t)$. The practical application requires caution. First, long trajectories (on the time scale of the lowest frequency components desired) are needed to calculate $C_{vv}(t)$ with adequate statistics. Second, relaxation phenomena in glass-like materials take place on the MD time scale, so that the MD sample will in general not be in thermal equilibrium. This is independent of the third problem of sample preparation mentioned above, and means that the PDOS can be more diffuse than in a well-equilibrated sample. The MD sample is usually quenched much faster than the samples on which inelastic neutron-scattering experiments are performed. Coordination defects can leave a distinct mark in the vibrational spectrum when their concentration is high enough.[1]

In spite of these reservations, the PDOS derived from our *a*-P trajectories 1 and 2 give valuable insight (see Figs. 9). Unlike the experimental spectrum for bulk *a*-P (Ref. 33, not shown), which follows closely the curve for *m*-P, our PDOS differs from both *m*- and *o*-P. However, the overall structure [Figs. 9(b) and 9(c)] — a broad low-frequency band at $\sim 50-250$ cm^{-1}, a distinct (though not a true) gap at 280 cm^{-1} followed by a narrower optical band up to ~ 500 cm^{-1} — is much more similar to the *o*-P spectrum. Although the relative intensities do not agree well for the above-stated reasons, there are four peaks and/or shoulders in the acoustic and two in the optical region as in *o*-P. More significantly, the pseudogap in *m*-P at 160 cm^{-1} has no analog in our theoretically derived spectrum. When optimally aligned, the MD spectra are redshifted by about 40 cm^{-1} from the experimental curve for *o*-P, due in part to the use of the s-nonlocality approximation. The changes in the PDOS of the first [Fig. 9(b)] and second, annealed trajectory [Fig. 9(c)] can be compared with Raman spectra of *a*-P thin films deposited at successively higher surface temperatures.[27] Although our MD derived spectra do not show a pseudogap opening at $\sim$160 cm^{-1}, we can observe changes in the high-frequency band that were taken as indicating a transition from layerlike to tubelike structure in Ref. 27. The highest frequency peak shifts from 385 cm^{-1} to 395 cm^{-1} upon annealing, and an additional strong peak appears at 355 cm^{-1}. Very similar changes occur in the corresponding regions of the high-frequency Raman band when the surface deposition temperature of *a*-P thin films in increased from 300 K to 510 K.

Our observation that fast-quenched *a*-P has a vibrational spectrum more similar to the orthorhombic modification than to the monoclinic is consistent with Raman-scattering experiments on *a*-P thin films.[27] This degree of similarity has been obtained, however, in an MD sample with little resemblance to the double layers of six rings in *o*-P. It can therefore be questioned whether the — admittedly stronger — similarity between the PDOS of slowly annealed *a*-P thin films, bulk *a*-P and *m*-P, is compelling evidence for more than a loose structural similarity.

IV. CONCLUSIONS

The determination of the structures of disordered materials is experimentally very difficult. Theoretical work is an essential complement, and we have performed here a detailed study of amorphous phosphorus. The method — molecular dynamics based on energy surfaces and forces calculated using density-functional theory — has been applied previously with success to determine the structures of the most stable isomers of phosphorus clusters. In *a*-P, we used the structures obtained from our MD simulation and from these P_n isomers to derive distribution functions of various kinds as well as phonon densities of states. We have found that the structure of rapidly quenched *a*-P resembles a network of the cluster structures found in our earlier work more closely than any of the crystalline forms of phosphorus. The existence of a network of molecular units (P_4Se_3) has been found experimentally in glassy P_xSe_{1-x}, and the present calculations show that a similar situation can arise in a one-component system. We anticipate that much of our discussion should also apply to *a*-As, and we are currently extending the work to a study of liquid phosphorus.

ACKNOWLEDGMENTS

We thank R. Car and M. Parrinello for valuable discussions, and S. Wilson for help with various phosphorus crystal structures. The calculations were performed on the Cray Y-MP 8/832 of the German Supercomputer Center HLRZ in the Forschungszentrum Jülich and the Cray-2 at the National Center for Supercomputing Applications (NCSA).

*Permanent address: Institut für Festkörperforschung, Forschungszentrum Jülich, D-5170 Jülich, Federal Republic of Germany.

[1] D. Hohl and R.O. Jones, Phys. Rev. B **43**, 3856 (1991).
[2] G.N. Greaves, S.R. Elliott, and E.A. Davis, Adv. Phys. **28**, 49 (1979).
[3] K. Kawashima, H. Hosono, Y. Abe, S. Fujitsu, and H. Yanagida, J. Non-Cryst. Solids **95&96**, 741 (1987).
[4] R.T. Phillips and Z. Sobiesierski, J. Phys. C **20**, 4259 (1987); Z. Sobiesierski and R.T. Phillips, J. Non-Cryst. Solids **90**, 457 (1987); R.T. Phillips, Z. Sobiesierski, W.T. Toner, J.R.M. Barr, and A.J. Langley, Solid State Commun. **63**, 481 (1987).
[5] G. Fasol, J. Phys. C **18**, 1729 (1985).
[6] S. Depinna and B.C. Cavenett, J. Phys. C **16**, 7063 (1983).
[7] This notation indicates fourfold- and twofold-coordinated pnictide atoms and should not to be confused with the chemical symbols P_n for n atomic phosphorus clusters.
[8] S.R. Elliott and E.A. Davis, J. Phys. C **12**, 2577 (1979); J. Non-Cryst. Solids **35&36**, 849 (1980).
[9] J. Donohue, *The Structures of the Elements* (Wiley, New York, 1974), Chap. 8.
[10] R.O. Jones and D. Hohl, J. Chem. Phys. **92**, 6710 (1990) (P_n clusters).

[11] R.O. Jones and D. Hohl, in *NATO Advanced Study Institute on Computer Simulations in Material Science: Interatomic Potentials, Simulation Techniques and Applications*, Vol. 205 of *NATO Advanced Study Institute, Series E; Applied Physics*, edited by M. Meyer and V. Pontikis (Kluwer Academic, Dordrecht, 1991), pp. 437–450.
[12] R.O. Jones and D. Hohl (unpublished) (As_n clusters).
[13] J. Hafner, Phys. Rev. Lett. **62**, 784 (1989) (MD study of liquid As).
[14] X.-P. Li, Phys. Rev. B **41**, 8392 (1990) (MD-DF study of liquid As).
[15] D.E.C. Corbridge, *Phosphorus. An Outline of its Chemistry, Biochemistry and Technology* (Elsevier, Amsterdam, 1985).
[16] J.R. Granada and J.C. Dore, Mol. Phys. **46**, 757 (1982).
[17] H. Thurn and B. Krebs, Acta Crystallogr. Sect. B **25**, 125 (1969).
[18] D.J. Verral and S.R. Elliott, Phys. Rev. Lett. **61**, 974 (1988).
[19] R.T. Phillips, D. Wolverson, M.S. Burdis, and Y. Fang, Phys. Rev. Lett. **63**, 2574 (1989).
[20] K. Krebs and H.U. Gruber, Z. Naturforsch. Teil A **22**, 96 (1967).
[21] H.U. Beyeler and S. Vepřek, Philos. Mag. B **41**, 327 (1980).
[22] F. Gompf and J.S. Lannin, J. Phys. (Paris) Colloq. **42**, C6-28 (1981).
[23] B.V. Shannabrook and J.S. Lannin, Phys. Rev. B **24**, 4771 (1981).
[24] J.S. Lannin, B.V. Shannabrook, and F. Gompf, J. Non-Cryst. Solids **49**, 209 (1982).
[25] G. Fasol, M. Cardona, W. Hönle, and H.G. von Schnering, Solid State Commun. **52**, 307 (1984).
[26] D.J. Olego, J.A. Baumann, M.A. Kuck, R. Schachter, C.G. Michel, and P.M. Raccah, Solid State Commun. **52**, 311 (1984).
[27] D.J. Olego, J.A. Baumann, and R. Schachter, Solid State Commun. **53**, 905 (1985).
[28] S.R. Elliott, J.C. Dore, and E. Marseglia, J. Phys. (Paris) Colloq. **46**, C8-349 (1985).
[29] E. Belin, C. Sénémaud, and A. Szàsz, Philos. Mag. B **58**, 551 (1988).
[30] G.E. Jellison, Solid State Commun. **30**, 481 (1979).
[31] R. Bellissent and G. Tourand, J. Phys. (Paris) **37**, 1423 (1976) (amorphous As).
[32] R. Bellissent, C. Bergman, R. Ceolin, and J.P. Gaspard, Phys. Rev. Lett. **59**, 661 (1987) (liquid As).
[33] F. Gompf, G. Fasol, M. Cardona, W. Hönle, and J.B. Suck, in *Proceedings of the 2nd International Conference on Phonon Physics, Budapest, Hungary, 1985*, edited by J. Kollár, N. Kroó, N. Menyhárd, and S. Siklós (World Scientific, Singapore, 1986).
[34] P. Briddon and R. Jones, J. Phys. Condens. Matter **1**, 10 361 (1989).
[35] R. Car and M. Parrinello, Phys. Rev. Lett. **55**, 2471 (1985); **60**, 204 (1988) (amorphous Si); I. Štich, R. Car, and M. Parrinello, *ibid.* **63**, 2240 (1989) (liquid Si).
[36] A detailed analysis can be found in G. Pastore, E. Smargiassi, and F. Buda, Phys. Rev. A **44**, 6334 (1991).
[37] D. Hohl, R.O. Jones, R. Car, and M. Parrinello, Chem. Phys. Lett. **139**, 540 (1987) (Se_n clusters).
[38] D. Hohl, R.O. Jones, R. Car, and M. Parrinello, J. Chem. Phys. **89**, 6823 (1988) (S_n clusters).
[39] D. Hohl, R.O. Jones, R. Car, and M. Parrinello, J. Am. Chem. Soc. **111**, 825 (1989) (S_7O).
[40] R.O. Jones and D. Hohl, J. Am. Chem. Soc. **112**, 2590 (1990) (Se_xS_y molecules).
[41] G. Galli, R.M. Martin, R. Car, and M. Parrinello, Phys. Rev. B **42**, 7470 (1990); Science **256**, 1547 (1990) (amorphous and liquid C).
[42] Q.-M. Zhang, G. Chiarotti, A. Selloni, R. Car, and M. Parrinello, Phys. Rev. B **42**, 5071 (1990) (liquid GaAs).
[43] F. Ancilotto, W. Andreoni, A. Selloni, R. Car, and M. Parrinello, Phys. Rev. Lett. **65**, 3148 (1990) [Si(111) surface].
[44] R.O. Jones and D. Hohl, Phys. Scri. **T35**, 154 (1991).
[45] R.O. Jones and D. Hohl, Int. J. Quantum Chem.: Quantum Chem. Symp. **24**, 141 (1990) (S_8, S_7O, and O_8).
[46] G.B. Bachelet, D.R. Hamann, and M. Schlüter, Phys. Rev. B **26**, 4199 (1982).
[47] For a review, see R.O. Jones and O. Gunnarsson, Rev. Mod. Phys. **61**, 689 (1989).
[48] I. Štich, R. Car, M. Parrinello, and S. Baroni, Phys. Rev. B **39**, 4997 (1989).
[49] Note that the MD-DF cluster calculations reported in Refs. 10 and 11 were performed using *sp* nonlocality in the pseudopotential and are not affected by the shift of interatomic distances towards larger r observed with the cruder approximation of s nonlocality.
[50] W.D. Luedtke and U. Landman, Phys. Rev. B **40**, 1164 (1989).
[51] V.A.Polukhin and M.M. Dzugotov, Phys. Met. Metall. **51**, 50 (1981).
[52] J. Hafner and W. Jank, Phys. Rev. B **42**, 11 530 (1990). This reference and Ref. 54 employ interatomic pair potentials derived from LDF calculations. Many structural data agree very well with a full MD-DF calculation when such parametrization is used in a consistent fashion.
[53] R.O. Jones, Phys. Rev. Lett. **67**, 224 (1991).
[54] W. Jank and J. Hafner, Phys. Rev. B **41**, 1497 (1990).
[55] X.-P. Li (private communication).

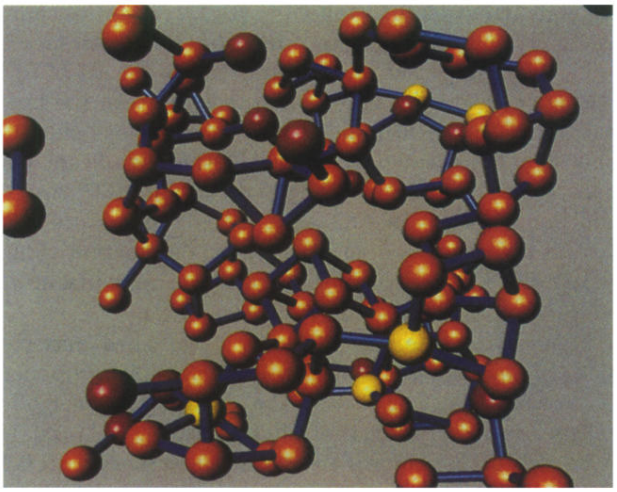

FIG. 4. Ball-and-stick model of a typical spatial configuration in a-P (trajectory 2). Twofold-coordinated defects are shown in red, fourfolds in yellow. All atoms inside the periodically repeated cube are shown and bonds are drawn between atoms within the cell with separation $d \leq 5.0$ a.u. Bonds to atoms in neighboring cells are omitted, so that the number of sticks is not necessarily a measure of the coordination number near the cell edges.

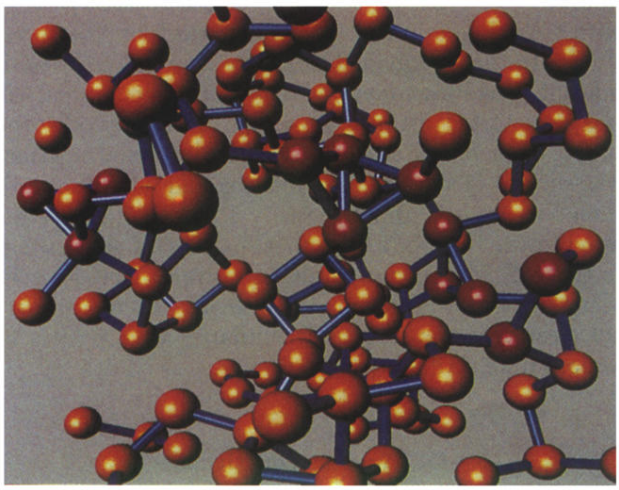

FIG. 6. Another view of the same configuration as in Fig. 4 from a similar angle. Atoms involved in near 60° bond angles are red, all others orange. Triangular P_3 and roof-shaped P_4 fragments and not P_4 tetrahedra are responsible for the peak at 60° in $A(\alpha)$.

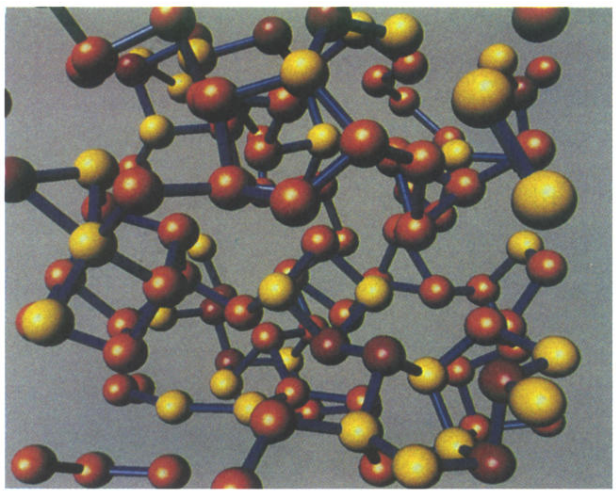

FIG. 8. Another view of the same configuration as in Fig. 4. All atoms connecting pyramids at angles $\phi = 160° - 180°$ are shown in red, the terminal atoms connected directly to those in yellow. Note the two closest full-trans conformations in the lower right-hand corner. Only the 124 atoms in the central unit cell are included.